Investigating the Impact of Soil Moisture on Thermal Infrared Emissivity Using ASTER Data

Heshun Wang, Qing Xiao, Hua Li, Yongming Du, and Qinhuo Liu

***Abstract*—This study investigates the effects of soil moisture (SM) on land surface emissivity (LSE) using the Advanced Spaceborne Thermal Emission and Reflection Radiometer (ASTER) LSE data acquired in Heihe Watershed Allied Telemetry Experimental Research (HiWATER). Three bare surface sites with automatic meteorological stations that collected long-term SM data were chosen to evaluate the SM impact. The ASTER LSE retrieval was performed using the water vapor scaling method to improve the atmospheric correction results, and the validation results indicate that the emissivity uncertainties are better than 1%. The multitemporal LSE data reveal that there is an increase in the emissivity with increasing SM. A logarithmic linear relationship was established to describe the broadband emissivity dependence with SM over each site, with determination coefficients of 0.9429, 0.7705, and 0.4603. The modeled values calculated using coefficients derived in previous studies for samples with similar compositions yielded good agreements with ASTER broadband emissivities over two sites. The empirical model also shows that the diurnal variation in emissivity, particularly over one site, is so significant that it should not be neglected.**

***Index Terms*—Advanced Spaceborne Thermal Emission and Reflection Radiometer (ASTER), emissivity, Heihe Watershed Allied Telemetry Experimental Research (HiWATER), soil moisture (SM), thermal infrared (TIR).**

I. Introduction

LAND surface emissivity (LSE) is a basic parameter in surface–atmosphere interaction processes and plays an important role in deriving land surface temperature (LST), as well as long-wave energy budget estimates. As an intrinsic property of natural materials, the LSE is always regarded as an indicator for the surface composition and is widely used in mineral mapping and studies of soil erosion [1].

In a typical land cover, water and dense vegetation have a stable high emissivity in the thermal infrared (TIR) region, whereas bare surface has relatively low emissivity, which varies with the spectral wavelength, viewing angle, surface roughness, soil moisture (SM), and composition. Laboratory and field measurements have revealed that SM has a significant effect on the LSE, particularly in the 8–9.5-μm region [2], [3]. To investigate the influence of SM on emissivity, Mira *et al.* [4] performed a series of laboratory measurements under controlled conditions and found that the emissivity in the 8.2–9.2-μm range could increase up to 16% for sandy soils, and then the authors determined a logarithmic dependence of TIR emissivity on SM [5]. The impact of SM on the LSE was well known from ground-based experiments; however, studies using remote sensing data to analyze this effect have been limited. Hulley *et al.* [6] found that the LSE increased 0.08–0.3 at 8.6 μm and up to 0.03 at 11 μm in the MODIS v4 and AIRS LSE products due to rainfall events over the Namib Desert. In addition, the LSE has been used to estimate the SM. Furthermore, Sobrino *et al.* [7] proposed an empirical method to estimate the SM, in which the emissivity worked as a regression parameter along with the LST and the normalized difference vegetation index. Both the laboratory measurements and the remote sensing observations indicated that the SM has large temporal and spatial variation and that the SM effects on the LSE should be taken into account to improve the accuracy of long-wave energy balance models.

The objective of this study is to investigate the SM impact on the TIR emissivity using the Advanced Spaceborne Thermal Emission and Reflection Radiometer (ASTER) data acquired in Heihe Watershed Allied Telemetry Experimental Research (HiWATER) [8] and then analyzing the emissivity difference between day and night due to the SM variation based on the empirical model derived from ASTER LSE data.

II. Experimental Data

A. HiWATER Experiment

HiWATER was designed as a watershed-scale campaign to enhance the applicability of remote sensing in integrated ecohydrological studies [8]. The experiment has taken place in the Heihe River Basin in an arid region of northwest China (see Fig. 1). Multiple-scale observations were performed in HiWATER [9], and significant improvements have been made through the use of many ground-based measurements via the wireless sensor network and automatic meteorological stations (AMSs) in conjunction with airborne and satellite observations. Additionally, field emissivity measurements were also performed to validate the satellite products.

B. AMS Site Descriptions

To evaluate the effect of SM on the bare surface emissivity, three AMS sites located in an exposed area were chosen in

Manuscript received February 1, 2014; May 1, 2014 and May 30, 2014; accepted June 30, 2014. This work was supported in part by the National Natural Science Foundation of China under Grant 91125003 and Grant 41101325, by the National Basic Research Program of China under Grant 2013CB733401, and by the National High-Technology Research and Development Program of China under Grant 2012AA12A303. *(Corresponding author: Qing Xiao.)*

H. Wang is with the State Key Laboratory of Remote Sensing Science, Institute of Remote Sensing and Digital Earth, Chinese Academy of Sciences, Beijing 100101, China, and also with the University of Chinese Academy of Sciences, Beijing 100049, China (e-mail: heshun8336@163.com).

Q. Xiao, H. Li, Y. Du, and Q. Liu are with the State Key Laboratory of Remote Sensing Science, Institute of Remote Sensing and Digital Earth, Chinese Academy of Sciences, Beijing 100101, China (e-mail: xiaoqing@radi.ac.cn; lihua@radi.ac.cn; duym@radi.ac.cn; liuqh@radi.ac.cn).

Color versions of one or more of the figures in this paper are available online at http://ieeexplore.ieee.org.

Digital Object Identifier 10.1109/LGRS.2014.2336912

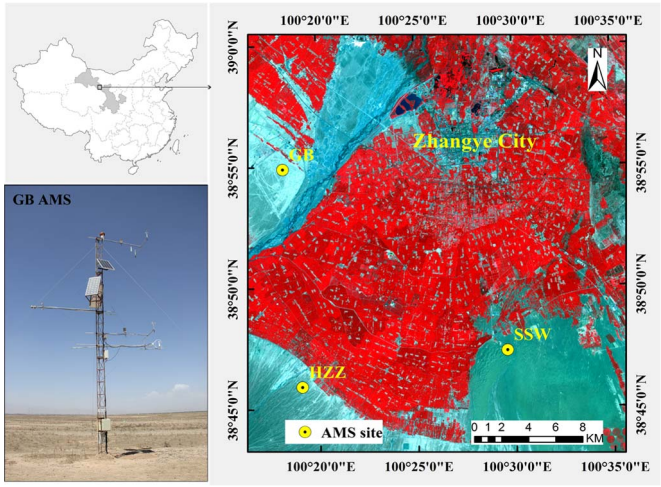

Fig. 1. Locations of the three bare surface sites with AMS. The upper-left image is the position of the study area in China, and the upper-right image is an ASTER false-color VNIR image of the area on July 10, 2012. The lower-left image is the photograph of the AMS at the GB site.

TABLE I
DESCRIPTIONS OF THE THREE AMS SITES AND THE MAIN SOIL PROPERTIES OF EACH SITE

	AMS Sites		
	GB	HZZ	SSW
Location	100.304 E, 38.915 N	100.319 E, 38.765 N	100.493 E, 38.789 N
Land cover	Gobi	Desert steppe	Sand dune
Texture (USDA)	Silt loam	Silt loam	Sand
Sand (%)	35.1	25.9	99.3
Silt (%)	63.1	72.2	0.7
Clay (%)	1.8	1.9	0.0
OM (%)	0.56	0.86	0.25
BD (g/cm^3)	1.42	1.46	1.53
Quartz (%)	48	41	71
Albite (%)	15	16	15
Microcline (%)	9	6	4
Clinochlore (%)	8	10	5
Muscovite (%)	6	7	2
Calcite (%)	9	14	3
Dolomite (%)	5	6	--
SM Sensor	CS616, Campbell		
SM Duration	06/08/2012 – 09/29/2012		

this study. The positions and descriptions of these sites can be found in Fig. 1 and Table I. The land cover types of these three sites are very representative of this region. The Gobi site (GB) consists of small grain size gravel, bare soil, and small *Alhagi sparsifolia*; the desert steppe site (HZZ) consists of bare soil and *Alhagi sparsifolia*; and the sand dune site (SSW) is more uniformly but sparsely covered by *Alhagi sparsifolia* [10]. The fraction of vegetation cover of these sites is less than 0.1, with little variation during the observation period.

The surface soil (0–5 cm) of these three sites was collected to determinate the key soil properties related to the SM and soil emissivity, including soil texture, bulk density (BD), organic matter content (OM), and mineral composition. The soil texture (proportions of sand, silt, and clay) was determined by a laser particle size analyzer, and the results showed that both the GB and HZZ sites are silt loam, whereas the SSW site is sand according to the USDA textural classification. X-ray diffraction

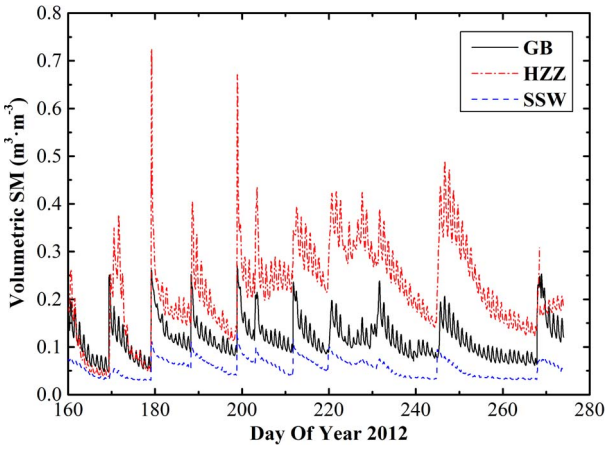

Fig. 2. Temporal evolution of SM measurements acquired by the reflectometers CS616 over each AMS from June 8 to September 20, 2012.

analyses show that quartz is the most abundant mineral in these soil samples, followed by albite; the percentages of each mineral are summarized in Table I.

The water content reflectometer CS616 (Campbell Scientific, USA), designed for long-term unattended water content monitoring, was installed in each AMS collecting SM data at seven different depths from 1 cm to 1 m. Because the TIR measurements are only sensitive to the top few micrometers of the surface, the data at 2-cm depth were used to represent the surface SM. The instrument based on the time-domain reflectometry could obtain the volumetric SM content with an uncertainty of $\pm 2.5\%$, and the data logger's sampling rate is six times per minute and records the average value every 10 min to eliminate the singular values.

The SM data of these three sites along the three months are illustrated in Fig. 2. The HZZ site had the highest SM levels, whereas the SSW site had the lowest. There are obvious fluctuations during this period, particularly around the rainfall events and the subsequent evaporation (see the sudden increases of SM in Fig. 2). This finding emphasizes the necessity to conduct the research of the influence of SM on the emissivity.

C. ASTER LSE

The ASTER sensor, onboard the Terra satellite, has five spectral bands in the TIR range (8–12 μm), with a spatial resolution of 90 m. To investigate the SM effect on the satellite-derived LSE, 12 clear-sky ASTER images, along with the MODIS atmospheric profile products (MOD07), were acquired over the experimental region from May 30 to September 28, 2012 (see Table II).

The standard ASTER LST and LSE products are generated by the temperature and emissivity separation (TES) algorithm [1]. Aside from the error induced by the soil-specific calibration of the empirical relationship of the TES algorithm, its accuracy is also limited by atmospheric correction errors of the satellite image. It is particularly true over gray bodies whose spectral contrast is so small that atmospheric uncertainties will magnify the minimum–maximum difference and lead to large LSE errors [11]. To solve this problem, the water vapor scaling (WVS) method was introduced to improve the results of the atmospheric correction in this study, which has previously been

TABLE II
LIST OF DATES AND OVERPASS TIMES OF THE ASTER DATA AND THE CORRESPONDING SM DATA AT THE THREE AMS SITES

Case	Date (month/ day/ year)	Overpass time (UTC)	Volumetric SM ($m^3 \cdot m^{-3}$)		
			GB	HZZ	SSW
1	05/30/2012	04:19			
2	06/15/2012	04:19	0.077	0.055	0.038
3	06/24/2012	04:13	0.089	0.091	0.033
4	07/10/2012	04:13	0.126	0.210	0.069
5	08/02/2012	04:19	0.139	0.310	0.076
6	08/11/2012	04:13	0.133	0.419	0.070
7	08/18/2012	04:19	0.218	0.338	0.072
8	08/27/2012	04:13	0.102	0.203	0.038
9	09/03/2012	04:19	0.170	0.409	0.072
10	09/12/2012	04:13	0.093	0.207	0.038
11	09/19/2012	04:19	0.083	0.155	0.034
12	09/28/2012	04:13	0.149	0.194	0.059

proven to be a valid approach [12]. Finally, the standard TES algorithm was adopted to retrieve the LSE.

For most land surface models, broadband emissivity (BBE) is an indispensable parameter. Therefore, this study focuses on the BBE dependence on SM. Cheng *et al.* [13] indicated that the BBE (8–13.5 μm) could be estimated from the ASTER narrowband emissivities using the following empirical equation:

$$\varepsilon_b = 0.197 + 0.025\varepsilon_{10} + 0.057\varepsilon_{11} + 0.237\varepsilon_{12} + 0.333\varepsilon_{13} + 0.146\varepsilon_{14} \quad (1)$$

where ε_b is the BBE, and ε_{10} to ε_{14} are the five ASTER narrowband emissivities.

III. RESULTS AND ANALYSIS

A. Evaluation of the Heterogeneity of the AMS Sites

There are observation-scale discrepancies between satellite and ground data. This arises because the footprint of ASTER is 90×90 m^2, whereas the AMS data only cover a single point. Before using the station data to represent the pixel value, the heterogeneity evaluation of the AMSs is indispensable. To inspect the subpixel distribution, the Thermal Airborne Spectrographic Imager (TASI) data with 9-m pixel size collected on July 10, 2012 was used to carry out this analysis. The TES algorithm was performed to retrieve the LSE product from the TASI data with 32 bands in the TIR domain [14]. These narrowband emissivities were convolved with the spectral response function of ASTER five TIR bands and then be converted to the BBE according to (1). Fig. 3 shows the TASI BBE in the 3×3 ASTER pixels and the histograms of the central ASTER pixel at the three sites as well as the mean and standard deviation values from TASI BBE. The standard deviations of these three sites (see Fig. 3) are all within the LSE accuracy (± 0.015) predicted by Gillespie *et al.* [1], which reveal that all the sites are homogeneous enough for this study.

B. ASTER Emissivity Validation

The ASTER LSE products were validated with the field measurements conducted by an ABB BOMEM MR304 Fourier transform infrared spectroscopy, which is a high-precision instrument with a spectral resolution of up to 1 cm^{-1} in the 2–15-μm range. Under field conditions, the targets and downward sky radiance were measured using the MR304 and a diffuse golden plate, and then, emissivity was retrieved by the iterative spectrally smooth temperature and emissivity separation algorithm, with accuracy better than 0.01 [3].

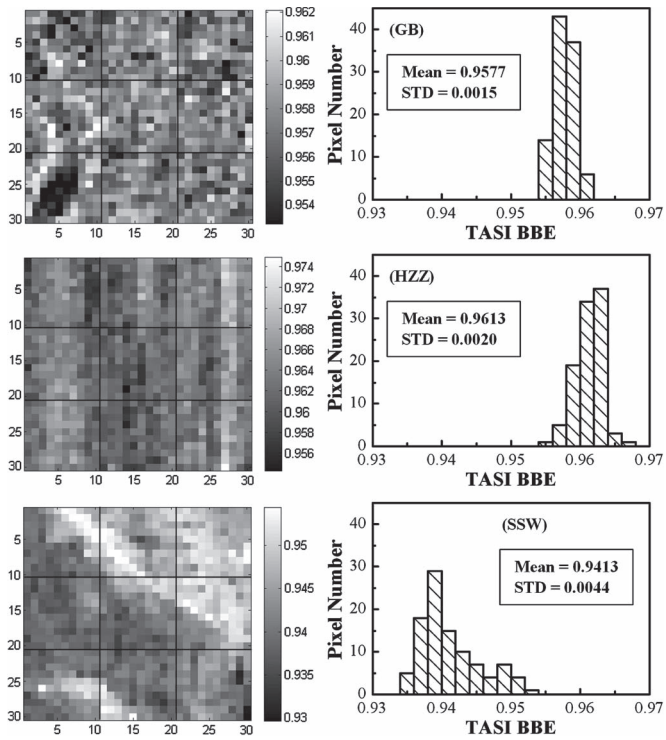

Fig. 3. TASI BBE data in the 3×3 ASTER pixels (left) and the histograms of the TASI BBE in the central ASTER pixel for the three sites on July 10, 2012.

The *in situ* measurements were performed at the HZZ and GB sites at 5:00 and 8:30 UTC on July 10, 2012, respectively. It was assumed that SM change from satellite overpass (4:13 UTC) was small, and considered small variation of emissivities, mostly of the GB sample. The SSW emissivity was measured along with the HZZ sample by *ex situ* means, because we considered that there are little emissivity differences between the disturbed and undisturbed sand samples. The ASTER LSE of these three sites on July 10, 2012 was compared with the field measured emissivity spectra convolved with the spectral response function of ASTER five TIR bands (see Fig. 4). The comparison results indicate that the TES algorithm works well for these bare surfaces with high spectral contrast. The absolute mean emissivity difference for all bands at the GB and HZZ sites are 0.003 and 0.0036, respectively, and 0.0079 for the SSW site.

C. ASTER Emissivity Dependence on SM

According to the SM data from the AMSs, the GB and SSW sites were more arid than the HZZ site, where the SM reached 0.4 $\mathrm{m}^3 \cdot \mathrm{m}^{-3}$ and fluctuated highly approximately 0.35 $\mathrm{m}^3 \cdot \mathrm{m}^{-3}$, which was mainly attributed to the soil texture. The HZZ site contains less sand and more silt, whereas SSW is almost sand. The SM variations created a distinct ASTER BBE increase of 0.03 during the study period, which cannot be neglected in calculating the net long-wave radiation.

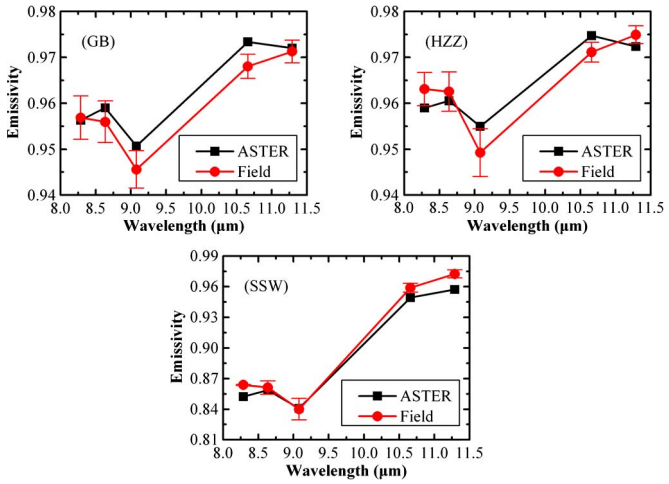

Fig. 4. Emissivity comparisons between ASTER LSE (July 10, 2012) and field measurement results (within 5 h after ASTER overpass) at the three AMS sites. The error bars denote the standard deviation of field measured emissivity.

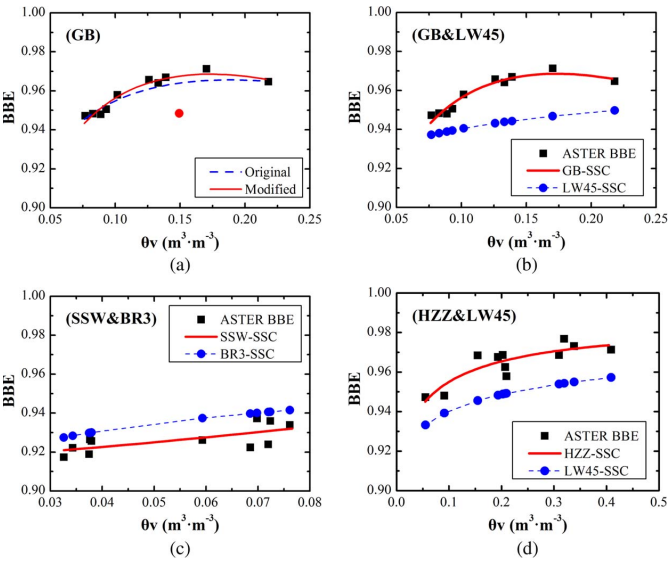

Fig. 5. ASTER BBE dependence on SM. (a) Empirical relationship derived from the GB site. The blue dash curve represents the regression using all 11 data, whereas the red one is the result with the problematic data (marked in red) excluded. (b)–(d) ASTER BBE dependence on SM (red curve) at the three sites and the modeled BBE value (blue points) using the SSC obtained from the samples with similar compositions in [5], which are summarized in Table III.

To quantitatively evaluate the SM effect on LSE, Mira *et al.* [5] determined a logarithmic dependence of TIR emissivity on SM from laboratory measurements following the equation:

$$\varepsilon_i = a_i + b_i\theta_v + c_i \ln(\theta_v) \tag{2}$$

where θ_v is the volumetric SM $(\mathrm{m}^3 \cdot \mathrm{m}^{-3})$; a, b, and c are the regression coefficients; and ε_i represents channel emissivity of the multichannel TIR radiometer CIMEL Electronique CE-312.

It is known that the emissivity dependence on SM differs among soil types. The three AMS sites with different texture and composition were evaluated applying (2), respectively.

For the GB AMS site, the determination coefficient (R^2) of (2) is 0.5989, which is largely affected by the data on September 28, 2012, which dramatically deviates from the fitting curve (see Fig. 5). The uncertainty of these data may be due to the error of the atmospheric compensation. With the removal of this singular data, the R^2 becomes 0.9429, and the coefficients are given in Table III.

TABLE III
COEFFICIENTS OF THE FITTING CURVE FOR GB, HZZ, AND SSW SITES AS WELL AS SAMPLE LW45 AND BR3 IN [5]

Samples	BBE = $a + b\cdot\theta_v + c\cdot\ln(\theta_v)$			
	a	b	c	R^2
GB	1.2351	-0.559	0.0968	0.9429
HZZ	0.9995	-0.0231	0.0183	0.7705
SSW	0.897	0.3262	-0.0039	0.4603
LW45	0.968	0	0.012	0.76
BR3	0.984	0	0.0165	0.93

The SM content at the HZZ site among the 11 images covered a wide range, and a robust fitting has been obtained (see Fig. 5 and Table III); the R^2 of the logarithmic regression is 0.7705.

Compared with the results of the GB site, the coefficients derived from HZZ are different to a certain extent. A main reason is (2) is soil composition dependent. The results reveal that GB emissivity increases faster than HZZ at low SM content for larger proportion of sand in the soil [4]. Another cause might due to the sample size being too small to construct a more robust regression.

The fitting results of the SSW site indicated that the R^2 value was a bit lower than the other two sites (see Table III), which could be attributed to the following two reasons. First, the sand has a low field capacity (around 0.1 $\mathrm{m}^3 \cdot \mathrm{m}^{-3}$), and the SM data synchronized with the ASTER data in this study have a small range of approximately 0.04 $\mathrm{m}^3 \cdot \mathrm{m}^{-3}$ (from 3.3% to 7.6%), whereas the SM uncertainty is up to $\pm 2.5\%$ according to the sensor manufacturer, which makes the construction of a robust relationship difficult. Second, similar to the GB site, the cause might be the uncertainty in the LSE products.

To evaluate the results in this study, the soil-specific coefficients (SSC) for the broadband channel (8.0–13.1 μm) of the CE312 radiometer derived from the samples with similar soil texture in [5] were used for analysis. Compared with the 14 soil samples mentioned in [5], GB and HZZ samples as well as sample LW45 in [5] are silt loam, and there is a sand sample labeled BR3 in [5] same as SSW. Their SSCs, specified in Table III, were adopted to calculate the modeled BBE and compared with the ASTER BBE of the three sites. The results are shown in Fig. 5. The modeled value using the LW45 SSC is lower than the BBE of the GB and HZZ sites, which might be attributed to the high quartz content (72.4%) in LW45. The soil texture of the HZZ sites is much closer to LW45, leading to better agreement with the increasing trend of LW45 than GB. Compared with the SSW sample, BR3 contains more OM (1.69%) and, hence, has larger emissivity, and the modeled values yield consistent results with the ASTER BBE at the SSW site. This study confirms that the emissivity-SM dependence previously inferred under laboratory conditions is also valid for the satellite data. However, the discrepancies do exist due to various factors, such as mineral compositions, LSE accuracy, and observation conditions.

It should be noted that SM is assumed to be the unique parameter attributing to the emissivity variation, and the effects of other factors are ignored. This is true for most situations in this study, because these sites have low fraction of vegetation

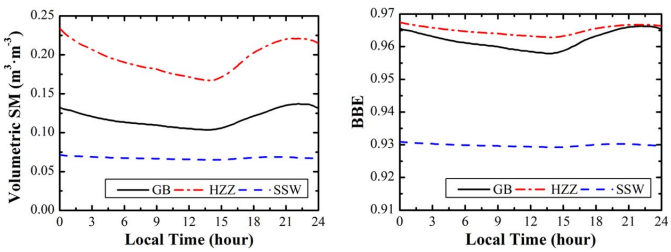

Fig. 6. SM diurnal variations on the three sites on July 10, 2012 and the corresponding BBE calculated by the empirical model derived from ASTER data in this letter (see Table III).

cover with little change, and the surface structures are rarely influenced by human activity.

D. Emissivity Diurnal Variation

Long-term SM observations also indicate that there are obvious variations between day and night for the 11 sunny days corresponding to the ASTER acquisitions. The maximum SM diurnal variations for the GB, HZZ, and SSW sites were 0.12, 0.16, and 0.02 $\mathrm{m}^3 \cdot \mathrm{m}^{-3}$, respectively. Based on the diurnal SM data of these 11 days, the corresponding BBE at the three sites was calculated by the empirical model coefficients (see Table III) derived from ASTER data in this letter. Fig. 6 shows the case on July 10, 2012. Considering the BBE differences between the time when the MODIS passed over during the day and night, the mean BBE differences between day and night of the 11 days for the GB, HZZ, and SSW sites are 0.01, 0.003, and 0.001. Despite with larger SM diurnal variation, the HZZ site has little BBE change for its much flatter BBE increase curve than the GB site. The BBE diurnal variation of specific soil such as GB is so distinct that might lead to a large error in the MODIS Day/Night LST inversion algorithm [15], in which the emissivity is assumed to be constant.

IV. Conclusion and Discussion

The ASTER data and long-term SM data of three bare surface sites were used in this study to investigate the dependence of the LSE on SM. To retrieve high-accuracy LSE data from the ASTER sensor, the WVS method has been introduced to improve the atmospheric correction result. Field emissivity measurements and higher spatial resolution airborne emissivity data showed that all these three sites yielded convincing results with LSE uncertainty less than 1% and were homogeneous enough for this study.

To investigate the dependence of BBE on SM, a soil-specific logarithmic empirical model derived from laboratory measurements was adopted. The data of the GB and HZZ sites yielded satisfying results, with determination coefficients of 0.9429 and 0.7705, respectively. The SSW site was slightly worse, which might due to the relatively small SM variation range and the emissivity uncertainty.

The soil-specific coefficients obtained from the soil samples in [5] with similar composition were used for comparison. There are discrepancies between the modeled values and ASTER BBE due to the differences of composition and observation scale; however, the BBE increase trend of HZZ and SSW sites yield good agreements with the laboratory results, which prove that the models inferred from the laboratory measurements are also valid for the satellite data.

In addition, the modeled BBE showed that the emissivity diurnal variation for specific soil is so significant that it should not be neglected in the day/night LST algorithm [15].

This study reveals the impact of SM on emissivity using ASTER LSE data, indicating the importance of the SM effect on BBE and the potential of SM inversion from satellite LSE products. However, only three bare surface sites were used, and the relationships were soil composition dependent. More surface types should be introduced in future research, and a general emissivity model independent of soil type is expected.

Acknowledgment

The authors would like to thank all the scientists, engineers, and students who participated in HiWATER campaigns and the two anonymous reviewers for their valuable comments and suggestions that have significantly improved this letter.

References

[1] A. Gillespie *et al.*, "A temperature and emissivity separation algorithm for Advanced Spaceborne Thermal Emission and Reflection Radiometer (ASTER) images," *IEEE Trans. Geosci. Remote Sens.*, vol. 36, no. 1, pp. 1113–1126, July 1998.

[2] J. W. Salisbury and D. M. D'Aria, "Infrared (8–14 μm) remote sensing of soil particle size," *Remote Sens. Environ.*, vol. 42, no. 2, pp. 157–165, Nov. 1992.

[3] Q. Xiao *et al.*, "A field measurement method of spectral emissivity and research on the feature of soil thermal infrared emissivity," *J. Infrared Millim. Waves*, vol. 22, no. 5, pp. 373–378, Oct. 2003.

[4] M. Mira, E. Valor, R. Boluda, E. Caselles, and C. Coll, "Influence of soil water content on the thermal infrared emissivity of bare soils: Implication for land surface temperature determination," *J. Geophys. Res.—Earth Surface*, vol. 112, no. F4, pp. 2003–2012, Dec. 2007.

[5] M. Mira *et al.*, "Soil moisture effect on thermal infrared (8–13-μm) emissivity," *IEEE Geosci. Remote Sens. Lett.*, vol. 48, no. 5, pp. 2251–2260, May 2010.

[6] G. C. Hulley, H. J. Hook, and A. M. Baldridge, "Investigating the effects of soil moisture on thermal infrared land surface temperature and emissivity using satellite retrievals and laboratory measurements," *Remote Sens. Environ.*, vol. 114, no. 7, pp. 1480–1493, Jul. 2010.

[7] J. Sobrino, B. Franch, C. Mattar, J. Jimenez-Munoz, and C. Corbari, "A method to estimate soil moisture from Airborne Hyperspectral Scanner (AHS) and ASTER data: Application to SEN2FLEX and SEN3EXP campaigns," *Remote Sens. Environ.*, vol. 117, pp. 425–428, Feb. 2012.

[8] X. Li *et al.*, "Heihe Watershed Allied Telemetry Experimental Research (HiWATER): Scientific objectives and experimental design," *Bull. Amer. Meteorol. Soc.*, vol. 94, no. 8, pp. 1145–1160, Aug. 2013.

[9] Z. Xu *et al.*, "Intercomparison of surface energy flux measurement systems used during the HiWATER—MUSOEXE," *J. Geophys. Res.—Atmos.*, vol. 118, no. 23, pp. 13140–13157, Dec. 2013.

[10] H. Li *et al.*, "Evaluation of the VIIRS and MODIS LST products in an arid area of Northwest China," *Remote Sens. Environ.*, vol. 142, pp. 111–121, Feb. 2014.

[11] C. Coll *et al.*, "Temperature and emissivity separation from ASTER data for low spectral contrast surfaces," *Remote Sens. Environ.*, vol. 110, no. 2, pp. 162–175, Sep. 2007.

[12] H. Tonooka, "Accurate atmospheric correction of ASTER thermal infrared imagery using the WVS method," *IEEE Trans. Geosci. Remote Sens.*, vol. 43, no. 12, pp. 2778–2792, Dec. 2005.

[13] J. Cheng, S. Liang, Y. Yao, and X. Zhang, "Estimating the optimal broadband emissivity spectral range for calculating surface longwave net radiation," *IEEE Geosci. Remote Sens. Lett.*, vol. 10, no. 2, pp. 401–405, Mar. 2013.

[14] H. Wang, Q. Xiao, H. Li, and B. Zhong, "Temperature and emissivity separation algorithm for TASI airborne thermal hyperspectral data," in *Proc. ICECC*, 2011, pp. 1075–1078.

[15] Z. Wan and Z. L. Li, "A physics-based algorithm for retrieving land-surface emissivity and temperature from EOS/MODIS data," *IEEE Trans. Geosci. Remote Sens.*, vol. 35, no. 4, pp. 980–986, Jul. 1997.